Author Manuscript

Author Manuscript

Author Manuscript

Author Manuscript

HHS Public Access

Author manuscript

*NMR Biomed*. Author manuscript; available in PMC 2019 July 01.

Published in final edited form as:

*NMR Biomed*. 2018 July ; 31(7): e3934. doi:10.1002/nbm.3934.

# Towards the complex dependence of $MTR_{asym}$ on $T_{1w}$ in amide proton transfer (APT) imaging

**Zhongliang Zu**[1,2]

[1]Vanderbilt University Institute of Imaging Science,

[2]Department of Radiology and Radiological Sciences

## Abstract

Amide proton transfer (APT) imaging is a variation of chemical exchange saturation transfer (CEST) MRI which has shown promise in diagnosing tumor, ischemic stroke, multiple sclerosis, and traumatic brain injury etc. Specific quantification of APT effect is crucial for the interpretation of APT contrast in pathologies. Conventionally, magnetization transfer ratio with asymmetric analysis ($MTR_{asym}$) has been used to quantify APT effect. However, some studies indicate that $MTR_{asym}$ is contaminated by water longitudinal relaxation time ($T_{1w}$) and thus it is necessary to normalize $T_{1w}$ in $MTR_{asym}$ to obtain specific quantification of APT effect. Until now, whether to use $MTR_{asym}$ or the $T_{1w}$ normalized $MTR_{asym}$ is still under debate in the field. In this paper, the influence of $T_{1w}$ on the quantification of APT was evaluated through theoretical analysis, numerical simulations, and phantom studies for different experimental conditions. Results indicate that there are two types of $T_{1w}$ effects ($T_{1w}$ recovery and $T_{1w}$-related saturation) which have inverse influences on the steady-state $MTR_{asym}$. In situations with no or weak direct water saturation (DS) effect, there is only $T_{1w}$ recovery effect and $MTR_{asym}$ linearly depends on $T_{1w}$. In contrast, in situations with significant DS effects, the dependence of $MTR_{asym}$ on $T_{1w}$ is complex, which is dictated by the competition of these two $T_{1w}$ effects. Therefore, by choosing appropriate irradiation powers, $MTR_{asym}$ could be roughly insensitive to $T_{1w}$. Moreover, in non-steady-state acquisitions with very short irradiation time, $MTR_{asym}$ is also roughly insensitive to $T_{1w}$. Therefore, for the steady-state APT imaging at high fields or with very low irradiation powers where there are no significant DS effects, it is necessary to normalize $T_{1w}$ to improve the specificity of $MTR_{asym}$. However, on clinical MRI systems (usually low fields or non-steady-state acquisitions), $T_{1w}$ normalization may not be necessary when appropriate sequence parameters are chosen.

## Graphical Abstract

Correspondence to: Zhongliang Zu, Ph.D., Vanderbilt University Institute of Imaging Science, 1161 21st Ave. S, Medical Center North, AAA-3112, Nashville, TN 37232-2310, zhongliang.zu@vanderbilt.edu, Phone: 615-875-9815, Fax: 615-322-0734, Grant Sponsor: R21 EB017873.

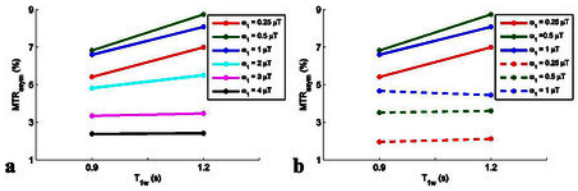

$MTR_{asym}$ from two creatine samples with pH 6.3 (mimicking amide) with different $T_{1w}$ shows that it has complex dependencies on $T_{1w}$. The steady-state $MTR_{asym}$ (a) are sensitive to $T_{1w}$ at relatively lower powers, but are roughly insensitive to $T_{1w}$ at relatively higher powers. The non-steady-state $MTR_{asym}$ (dashed line in (b)) are relatively insensitive to $T_{1w}$ compared with the steady-state $MTR_{asym}$ with the same powers (solid line in (b)).


### Keywords

MRI; chemical exchange saturation transfer (CEST); amide proton transfer (APT); $T_{1w}$ normalization


## INTRODUCTION

Chemical Exchange Saturation Transfer (CEST) is a sensitivity enhancement mechanism that has shown great potentials in imaging molecules in millimolar range (1–3). In CEST imaging, an irradiation RF pulse is applied at the frequency offset of exchangeable protons of solute molecules and the subsequent chemical exchange between those saturated protons and water protons reduces the magnitude of the measured water signal. Because water is significantly more abundant than the solutes, the detection sensitivity to exchanging protons by measuring water signal is magnified. Previously, CEST effects have been observed for a number of endogenous and exogenous molecules (4–12), and have been found to be sensitive to tissue pH (13,14). Amide proton transfer (APT) is an important application of CEST imaging, which detects the chemical exchange between backbone amide protons of proteins/peptides and water protons (14). In the last decade, APT has been applied to diagnose tumors (5,15–18), ischemic stroke (19–22), multiple sclerosis (23), and traumatic brain injury (24,25).

However, CEST is an indirect method to detect solute molecules or pH through measurements of water signals, and thus depends on multiple other tissue parameters including direct water saturation (DS), semi-solid magnetization transfer (MT), and water longitudinal relaxation time ($T_{1w}$). Those non-exchange related factors may vary in pathologies, which reduces the specificity of CEST imaging and may lead to misinterpretations. To remove contaminations from these factors, a reference signal that ideally has the same contributions from DS and semi-solid MT effects, but without chemical exchange, is required to compare to the exchange-labeled signal. Conventionally, the difference in the label and reference signals normalized to a control signal with no saturating pulses, termed CEST ratio (CESTR), was used to quantify the CEST effect. The CESTR was also named magnetization transfer ratio with asymmetric analysis ($MTR_{asym}$) when the reference signal is obtained from the offset frequency symmetric about the water resonance



Author Manuscript Author Manuscript Author Manuscript Author Manuscript

Author Manuscript Author Manuscript Author Manuscript Author Manuscript

(3). However, CEST, DS, and non-specific MT effects have mutual interactions, and do not add linearly (26). Thus CESTR cannot fully remove the DS and MT effects (26–28). Recently, Zaiss *et al.* introduced an alternative analysis of CEST data, which subtracts the reciprocals of the label and reference signals obtained in steady state and normalize water longitudinal relaxation time ($T_{1w}$), to address the non-specificities associated with CESTR. This method is termed apparent exchange-dependent relaxation (AREX) (26–28), and its specificity has been previously evaluated through simulations, phantom, and animal studies (26,29,30).

Although AREX is specific, it requires special hardware for long-time RF irradiation as well as measurement of water longitudinal relaxation time ($T_{1w}=1/R_{1w}$) which lengthen the total imaging time. Therefore, CESTR, as a simple and effective metric to remove most of the influence ($0^{th}$ order effect) from DS and semi-solid MT effects, is still widely used especially in clinical applications (31–35). However, the $T_{1w}$ normalization in AREX and a previous defined CESTR under weak saturation pulse approximation (3) suggest that CESTR depends on $T_{1w}$. This raises a concern whether there is a need to normalize $T_{1w}$ in CESTR.

Here, the influence of $T_{1w}$ on CESTR quantification of APT was evaluated through theoretical analysis, numerical simulations, and phantom studies for different experimental conditions. This study will provide insights into the specificity of APT imaging and guide MRI researchers and radiologists to choose appropriate CEST quantification metrics.

## THEORY

### Steady-state CESTR under an approximation of weak saturation pulse and complete saturation

CESTR is defined by (3),

$$CESTR(\Delta\omega) = \frac{S_{ref}(\Delta\omega) - S_{lab}(\Delta\omega)}{S_0} \quad (1)$$

where Δω is the RF frequency offset from water resonance frequency. $S_{lab}(\Delta\omega)$, $S_{ref}(\Delta\omega)$, and $S_0$ are the label, reference, and non-irradiated control signals, respectively. A previous study indicates that CESTR can be described by the following Eq. (2) under an approximation of weak saturation pulse and complete saturation, and also with spin system in steady state (3),

$$CESTR(\Delta\omega) = \frac{f_s k_{sw}}{R_{1w} + f_s k_{sw}} \quad (2)$$

where $f_s$ and $k_{sw}$ are the solute concentration and exchange rate, respectively. The steady-state acquisition can usually be obtained with RF irradiation time ($t_p$) > $5T_{1w}$. For slow exchanging pool ($f_s k_{sw} < R_{1w}$), Eq. (2) could be approximated by,

Author Manuscript Author Manuscript Author Manuscript Author Manuscript

$$CESTR(\Delta\omega) = \frac{f_s k_{sw}}{R_{1w}} \quad (3)$$

Eq. (3) suggests that $T_{1w}$ normalization is required in CESTR to obtain specific quantification of exchanging effect. However, under this weak saturation pulse approximate, there is no DS effect, and thus both Eq. (2) and Eq. (3) may be too simple to provide a correct $T_{1w}$ dependence for *in vivo* CESTR.

## Steady-state CESTR with DS and semi-solid MT effects

Zaiss *et al.* (26,27) have shown that water, chemical exchange, and semi-solid MT effects acquired in steady state can be described simultaneously by superimposing their rotating frame relaxations (when the exchanging solute concentration is much less than 1),

$$R_{1p}(\Delta\omega) \approx R_{eff}(\Delta\omega) + R_{ex}^{cest}(\Delta\omega) + R_{ex}^{MT}(\Delta\omega)/(1 + f_m) \quad (4)$$

where $R_{1\rho}(\Delta\omega)$, $R^{cest}_{ex}(\Delta\omega)$, and $R^{MT}_{ex}(\Delta\omega)$ are water longitudinal relaxation, chemical exchange, and semi-solid MT effects in the rotating frame, respectively; $f_m$ is the semi-solid component concentration. $R^{cest}_{ex}(\Delta\omega)$, $R_{eff}$, and $R_{1\rho}(\Delta\omega)$ can be described by the following Eq. (5), Eq. (6), and Eq. (7), respectively,

$$R_{ex}^{cest}(\Delta\omega) = \frac{f_s k_{sw} \omega_1^2}{\omega_1^2 + (R_{2s} + k_{sw})k_{sw} + (\Delta\omega - \Delta)^2 k_{sw}/(R_{2s} + k_{sw})} \quad (5)$$

$$R_{eff} = R_{1w}\cos^2\theta + R_{2w}\sin^2\theta \quad (6)$$

$$R_{1p}(\Delta\omega) \approx \frac{S_0 R_{1obs}}{S^{ss}(\Delta\omega)} \quad (7)$$

with

$$\cos^2\theta = \frac{\Delta\omega^2}{\omega_1^2 + \Delta\omega^2}; \qquad \sin^2\theta = \frac{\omega_1^2}{\omega_1^2 + \Delta\omega^2}$$

where $\omega_1$ is the RF irradiation power; $R_{2w}$ ($1/T_{2w}$) and $R_{2s}$ ($1/T_{2s}$) are the transverse relaxation rate of water and solute, respectively; $\Delta$ is solute resonance frequency; $S^{ss}(\Delta\omega)$ is the steady-state CEST signal which represents either $S_{lab}(\Delta\omega)$ or $S_{ref}(\Delta\omega)$; $R_{1obs}$ is the

Author Manuscript Author Manuscript Author Manuscript Author Manuscript

apparent water longitudinal relaxation rate in the presence of semi-solid MT effect, which can be obtained by $(R_{1w} + f_m R_{1m})/(1+f_m)$ in which $R_{1m}$ is the longitudinal relaxation rate of the semi-solid component (26). Here, $R^{cest}_{ex}$ can be looked as the product of $f_s$, $k_{sw}$, and labeling efficiency (27), which can represent pure CEST effect that depends only on solute exchanging parameters and sequence parameters but not non-specific tissue parameters. By substituting $R_{1\rho}(\Delta\omega)$ in Eq. (4) with Eq. (7), and expanding it in powers of $R^{cest}_{ex}(\Delta\omega)$, we can obtain,

$$\begin{aligned} S^{ss}(\Delta\omega) &\approx \frac{S_0 R_{1obs}}{R_{eff}(\Delta\omega) + R_{ex}^{MT}(\Delta\omega)/(1+f_m) + R_{ex}^{cest}(\Delta\omega)} \\ &\approx \frac{S_0 R_{1obs}}{R_{eff}(\Delta\omega) + R_{ex}^{MT}(\Delta\omega)/(1+f_m)} - \frac{S_0 R_{1obs} R_{ex}^{cest}(\Delta\omega)}{(R_{eff}(\Delta\omega) + R_{ex}^{MT}(\Delta\omega)/(1+f_m))^2} + \cdots \end{aligned} \quad (8)$$

In APT imaging in biological tissues, $R^{cest}_{ex}$ is much less than $R_{eff}$ (Sup. Table S1 shows the calculated $R^{cest}_{ex}$ with complete saturation ($=f_s k_{sw}$) and $R_{eff}$ for different experimental conditions using Eq. (5) and Eq. (6), respectively, with parameters mimicking amide and tissue water). Therefore, the first two items of the series in Eq. (8) dominate $S^{ss}$. Assuming $R^{cest}_{ex}(\Delta\omega)$ is zero in the reference signal, we can obtain $S_{ref}$ in steady state,

$$S_{ref}(\Delta\omega) \approx \frac{S_0 R_{1obs}}{R_{eff}(\Delta\omega) + R_{ex}^{MT}(\Delta\omega)/(1+f_m)} \quad (9)$$

By further substituting Eq. (1) with Eq. (8) and Eq. (9), we can derive CESTR for a more complex model with DS and semi-solid MT effects,

$$CESTR(\Delta\omega) \approx \frac{R_{1obs} R_{ex}^{cest}(\Delta\omega)}{(R_{eff}(\Delta\omega) + R_{ex}^{MT}(\Delta\omega)/(1+f_m))^2} \approx \frac{1}{R_{1obs}} \left(\frac{S_{ref}}{S_0}\right)^2 R_{ex}^{cest}(\Delta\omega) \quad (10)$$

From Eq. (8) and Eq. (10), we find that CESTR only removes the $0^{th}$ order term, but not higher order terms of the non-exchange related factors, which thus still depends on DS and semi-solid MT effects. Eq. (10) also provides an approximate model for the steady-state CESTR signal which shows the relationship between CESTR and the pure CEST effect quantified by $R^{cest}_{ex}$.

### Dependence of the steady-state CESTR with DS effect on $R_{1w}$.

To be simple, we ignore the semi-solid MT effect in Eq. (10). Then we substitute Eq (10) with Eq. (6), replace $R_{1obs}$ with $R_{1w}$, and obtain,

Author Manuscript Author Manuscript Author Manuscript Author Manuscript

$$CESTR(\Delta\omega) \approx \underbrace{\frac{1}{R_{1w}}}_{T_{1w}\ \text{recovery}} \left( \underbrace{\frac{\omega_1^2 + \Delta\omega^2}{\frac{R_{2w}}{R_{1w}}\omega_1^2 + \Delta\omega^2}}_{T_{1w}-\text{related saturation}} \right)^2 R_{ex}^{cest}(\Delta\omega) \quad (11)$$

Eq. (3) suggests that there is a $T_{1w}$ scaling effect under an approximation of weak saturation pulse. Since there are no DS and semi-solid MT effects in Eq. (3), the CESTR in Eq. (3) should be determined only by the decrease of water signal due to chemical exchange and the recovery of water signal due to $T_{1w}$. Thus we name this $T_{1w}$ effect in Eq. (3) as $T_{1w}$ recovery effect here. Furthermore, since $T_{1w}$ recovery exists in all spin systems, it should also present when there are DS and semi-solid MT effects. Therefore, the first item in Eq. (11) should represent the $T_{1w}$ recovery effect. By comparing Eq. (11) with Eq. (3), we find that except the $T_{1w}$ recovery effect, there is another $T_{1w}$ effect which indirectly influences CESTR through the DS effect. Here, we name this $T_{1w}$ effect as $T_{1w}$-related saturation effect. From Eq. (11), we also know that the two $T_{1w}$ effects have inverse influences on CESTR, which may result in different $T_{1w}$ dependence as that given by Eq. (3). The two competing $T_{1w}$ effects suggest that $T_{1w}$ normalization may not be generally required in CESTR. Eq. (11) also suggests that except $R_{1w}$, the DS effect also depends on $R_{2w}$ and $\Delta\omega/\omega_1$.

### Dependence of the non-steady-state CESTR on $R_{1w}$

The non-steady-state CEST signals ($t_p << 5T_{1w}$) with long recovery time ($t_{rec} > 5T_{1w}$, $t_{rec}$ is the recovery time between the end the acquisition module and the beginning of next RF irradiation pulse) were previously described by (27,36),

$$\frac{S^{nss}(\Delta\omega)}{S_0} = (1 - \frac{S^{ss}}{S_0})\exp(-R_{1\rho}t_p) + \frac{S^{ss}}{S_0} \quad (12)$$

where $S^{nss}$ is the water signal acquired in the non-steady-state CEST imaging.

In some non-steady-state CEST imaging especially in clinic, both $t_p$ (usually from 200 ms to 1000 ms) and $t_{rec}$ (~2 s) are less than $5T_{1w}$ (31–35). As a result: (1) the control scan will obtain a non-equilibrium signal ($S_{unsat}$) which is less than $S_0$; (2) the initial signal before the RF irradiation ($S_i$) is not equal to $S_0$ (37). In this case, Eq. (12) becomes,

$$\frac{S^{nss}(\Delta\omega)}{S_{unsat}} = (\frac{S_i}{S_{unsat}} - \frac{S^{ss}}{S_{unsat}})\exp(-R_{1\rho}t_p) + \frac{S^{ss}}{S_{unsat}} \quad (13)$$

Eq. (13) can be rewritten as

Author Manuscript Author Manuscript Author Manuscript Author Manuscript

$$\frac{S^{\mathrm{nss}}(\Delta\omega)}{S_{unsat}} = \left(\left(\frac{S_i}{S_0} - \frac{S^{ss}}{S_0}\right)\exp\left(-R_{1\rho}t_p\right) + \frac{S^{ss}}{S_0}\right)\frac{S_0}{S_{unsat}} \quad (14)$$

When $t_p << 1/R_{1\rho}$,

$$\frac{S^{\mathrm{nss}}(\Delta\omega)}{S_{unsat}} = \left(\frac{S_i}{S_0} - \left(\frac{S_i}{S_0}\left(R_{eff}(\Delta\omega) + R_{ex}^{\mathrm{MT}}(\Delta\omega)\right) - R_{1w} + \frac{S_i}{S_0}R_{ex}^{cest}(\Delta\omega)\right)t_p\right)\frac{S_0}{S_{unsat}} \quad (15)$$

By assuming $R^{cest}_{ex}(\Delta\omega)$ is zero in the reference scan, the non-steady-state CESTR can be derived as,

$$CESTR(\Delta\omega) \approx \frac{S_i}{S_{unsat}}R_{ex}^{cest}(\Delta\omega)t_p \quad (16)$$

When $t_{rec} > 5T_{1w}$, $S_i = S_{unsat} = S_0$. Then CESTR = $R^{cest}_{ex}(\Delta\omega)t_p$ which is independent of $T_{1w}$. When $t_{rec} < 5T_{1w}$ and because $t_p << 5T_{1w}$, $S_i \approx S_{unsat} < S_0$. Then, CESTR could be also roughly independent of $T_{1w}$.

## METHODS

### Numerical simulations

Numerical simulations were used to evaluate these two competing $T_{1w}$ effects and to validate the approximate model given in Eq. (10) and Eq. (11). Two-pool (solute and water) model numerical simulations were performed with a continuous wave (CW) CEST sequence with a series of $\omega_1$ (1 μT, 2 μT, 3 μT, 4 μT, and 5 μT) and $T_{1w}$ (0.5 s, 1 s, 1.5 s, 2 s, and 2.5 s). The irradiation time is 8 s for steady states and 0.5 s for non-steady states. Table 1 lists the simulation parameters mimicking APT imaging. All CESTR were calculated by using the asymmetric analysis. So in following sections, we use $MTR_{asym}$ to represent CESTR.

**(a)** To study the $T_{1w}$ recovery effect in Eq. (10) and Eq. (11) separately, we plotted the steady-state $MTR_{asym}$ vs. $T_{1w}$ with Δω set to be $100\omega_1$ to satisfy the condition of $\omega_1 << \Delta\omega$. We also plotted $1/R_{1w}$ vs. $T_{1w}$ in the same figure and scaled it for comparison with the curve of $MTR_{asym}$ vs. $T_{1w}$.

**(b)** To study the $T_{1w}$-related saturation effect in Eq. (10) and Eq. (11) separately, we plotted the steady-state $MTR_{asym}\cdot R_{1w}$ vs. $T_{1w}$ with: (1) Δω set to be $10\omega_1$, $5\omega_1$, and $2\omega_1$ with $T_{2w}$ of 50 ms, respectively; (2) $T_{2w}$ set to be 10 ms, 30 ms, 50 ms, 70 ms, 100 ms, and 150 ms with $\Delta\omega/\omega_1$ of 5, respectively. The product of $MTR_{asym}$ and $R_{1w}$ was used to remove the $T_{1w}$ recovery effect so that it only shows the $T_{1w}$-related saturation effect. $(S_{ref}/S_0)^2$ vs. $T_{1w}$ was also plotted in the same figure and scaled for comparison with the curve of $MTR_{asym}\cdot R_{1w}$ vs. $T_{1w}$. $(S_{ref}/S_0)^2$ was obtained through numerical simulations with RF offset symmetric about the water resonance against CEST effects.

Author Manuscript Author Manuscript Author Manuscript Author Manuscript

**(c)** To study how the two $T_{1w}$ effects in Eq. (10) and Eq. (11) influence the steady-state $MTR_{asym}$, we plotted the steady-state $MTR_{asym}$ vs. $T_{1w}$ with: (1) $\Delta\omega$ set to be $10\omega_1$, $5\omega_1$, and $2\omega_1$ with $T_{2w}$ of 50 ms, respectively; (2) $T_{2w}$ set to be 10 ms, 30 ms, 50 ms, 70 ms, 100 ms, and 150 ms with $\Delta\omega/\omega_1$ of 5, respectively.

**(d)** To study whether the approximate model of $MTR_{asym}$ in Eq. (10) is valid, we compared the steady-state $MTR_{asym}$ with $(S_{ref}/S_0)^2 R^{cest}_{ex}/R_{1w}$ for different experimental conditions, in which the steady-state $MTR_{asym}$ and $(S_{ref}/S_0)^2$ were from simulations, and $R^{cest}_{ex}$ was calculated using Eq. (5) with the same parameters as those in the simulation.

**(e)** To study the dependence of the non-steady-state $MTR_{asym}$ in Eq. (16) on $T_{1w}$, we plotted the non-steady-state $MTR_{asym}$ vs. $T_{1w}$ with: (1) $\Delta\omega$ set to be $10\omega_1$, $5\omega_1$, and $2\omega_1$ with $T_{2w}$ of 50 ms, respectively; (2) $T_{2w}$ set to be 10 ms, 30 ms, 50 ms, 70 ms, 100 ms, and 150 ms with $\Delta\omega/\omega_1$ of 5, respectively. $t_p$ was 0.5 s for the non-steady-state acquisition. For the simulation of the non-steady-state acquisition with short recovery time, $t_{rec}$ was 1.5 s and the Z component of water signal before recovery was set to 0 by assuming a 90° excitation for the readout.

The coupled Bloch equations can be written as $\frac{d\mathbf{M}}{dt} = \mathbf{AM} + \mathbf{M}_0$, where A is a 6 × 6 matrix for the two-pool model. The water and solute pools each has three coupled equations representing their x, y, and z components. All numerical calculations of CEST signals integrated the differential equations through the sequence using the ordinary differential equation solver (ODE45) in MATLAB 2014a (Mathworks, Natick, MA, USA).

## Sample preparation and MRI

Two creatine samples served to evaluate the dependence of $MTR_{asym}$ on $T_{1w}$. Creatine was added to phosphate-buffered saline (PBS) solution to reach a concentration of 100 mM, and the pH of the solution was titrated to 6.3 by using NaoH/HCl. The solution was then transferred into two tubes. 0.075 mM and 0.05 mM $MnCl_2$ were added to the two tubes (samples #1 and #2), respectively, to vary $T_{1w}$. At room temperature and with pH of 6.3, creatine is in the slow exchange regime (38,39). The resonance frequency offsets of creatine amines and protein amides are at around 1.9 ppm and 3.5 ppm, respectively. So the Δ of creatine at 4.7 T (380 Hz) is close to that of amide at 3 T (447 Hz). Therefore, experiments on creatine at 4.7 T can be used to mimic amide at clinical 3 T.

All measurements on creatine samples were performed at a Varian 4.7 T MRI system with a 38-mm Doty coil (Doty Scientific Inc. Columbia, SC, USA) for both transmission and reception. CEST measurements were performed by applying a CW RF irradiation before free induction decay (FID) acquisition. An 8-s irradiation pulse was performed for steady-state acquisitions, and a 0.5-s irradiation pulse was performed for non-steady-state acquisitions. TR was 10 s for both the steady-state acquisition and the non-steady-state acquisition. $S_{lab}$, $S_{ref}$, and $S_0$ were acquired with RF offsets at 1.9 ppm, −1.9 ppm, and 500 ppm, respectively. $MTR_{asym}$ was calculated using Eq. (1). $T_{1w}$ were obtained using an inversion recovery sequence. $T_{2w}$ were obtained using a multiple echo sequence.

Author Manuscript Author Manuscript Author Manuscript Author Manuscript

## RESULTS

### $T_{1w}$ recovery effect and $T_{1w}$-related saturation effect

Fig. 1 shows the simulated steady-state $MTR_{asym}$ vs. $T_{1w}$ for the condition of $\omega_1 << \Delta\omega$ (no DS effect). Note that the curves of $MTR_{asym}$ vs. $T_{1w}$ match the curve of $1/R_{1w}$ vs. $T_{1w}$, indicating that $MTR_{asym}$ linearly depends on $T_{1w}$, which confirms the presence of the $T_{1w}$ recovery effect. Fig. 2 shows the simulated steady-state $MTR_{asym}R_{1w}$ vs. $T_{1w}$ for a series of $\Delta\omega/\omega_1$ (with DS effect) and $T_{2w}$. Note that different from Fig. 1, $MTR_{asym}R_{1w}$ in Fig. 2 inversely depends on $T_{1w}$, suggesting the presence of other $T_{1w}$ effects. Also note that the curves of $MTR_{asym}R_{1w}$ vs. $T_{1w}$ match the curve of $(S_{ref}/S_0)^2$ vs. $T_{1w}$, indicating that $MTR_{asym}R_{1w}$ may depend on DS effect regulated by $T_{1w}$, which confirms the presence of $T_{1w}$-related saturation effect. It was also found that both $MTR_{asym}R_{1w}$ and $(S_{ref}/S_0)^2$ values are smaller for lower $\Delta\omega/\omega_1$ values (see Fig. 2a-2c) and shorter $T_{2w}$ values (see Fig. 2d-2i), suggesting that $MTR_{asym}R_{1w}$ also depends on DS effect regulated by $\Delta\omega/\omega_1$ and $T_{2w}$.

### Dependence of the steady-state $MTR_{asym}$ on $T_{1w}$ with DS effect.

Fig. 3 shows the simulated steady-state $MTR_{asym}$ vs. $T_{1w}$ for a series of $\Delta\omega/\omega_1$ and $T_{2w}$. Note that the curves of $MTR_{asym}$ vs. $T_{1w}$ are relatively flat in Fig. 3b and Fig. 3e-3h, suggesting that the two competing $T_{1w}$ effects may result in the rough independence of $MTR_{asym}$ on $T_{1w}$ by choosing appropriate sequence parameters. In Fig. 3a and 3i, $MTR_{asym}$ increases with $T_{1w}$ which is due to that the $T_{1w}$ recovery effect dominates the $T_{1w}$-related saturation effect when $\Delta\omega/\omega_1$ is relatively higher or $T_{2w}$ is relatively longer and thus the DS effect is relatively weaker. In Fig. 3c and 3d, $MTR_{asym}$ decreases with $T_{1w}$ which is due to that the $T_{1w}$-related saturation effect dominates the $T_{1w}$ recovery effect when $\Delta\omega/\omega_1$ is relatively lower or $T_{2w}$ is relatively shorter and thus the DS effect is relatively greater. Fig. 4 shows the measured steady-state $MTR_{asym}$ from two creatine samples with different $T_{1w}$. Note that the steady-state $MTR_{asym}$ increases with $T_{1w}$ with lower $\omega_1$, but becomes roughly insensitive to $T_{1w}$ with higher $\omega_1$.

### An approximate model of $MTR_{asym}$

Fig. 5 shows the simulated steady-state $MTR_{asym}$ and $(S_{ref}/S_0)\ {}^2R^{cest}_{ex}/R_{1w}$ vs. $T_{1w}$ and $\omega_1$ for a series of $\Delta\omega/\omega_1$ values and $T_{2w}$. The curves of $MTR_{asym}$ match the curves of $(S_{ref}/S_0)^2R^{cest}_{ex}/R_{1w}$ very well for all experimental conditions, confirming the approximate model in Eq. (10).

### Dependence of the non-steady-state $MTR_{asym}$ on $R_{1w}$

Fig. 6 shows the simulated non-steady-state $MTR_{asym}$ with full recovery ($t_p$ = 0.5 s) vs. $T_{1w}$ for a series of $\Delta\omega/\omega_1$ values and $T_{2w}$, respectively. Fig. 7 shows the simulated non-steady-state $MTR_{asym}$ with short recovery time ($t_p$ = 0.5 s, $t_{rec}$ = 1.5 s) vs. $T_{1w}$ for a series of $\Delta\omega/\omega_1$ values and $T_{2w}$, respectively. Note that the curves of $MTR_{asym}$ vs. $T_{1w}$ are relatively flat for all experimental conditions, indicating that $MTR_{asym}$ is roughly independent of $T_{1w}$ for the non-steady-state irradiation with very short irradiation time, which confirms Eq. (16). Fig. 8 shows the measured $MTR_{asym}$ from two creatine samples with different $T_{1w}$. Note that

Author Manuscript Author Manuscript Author Manuscript Author Manuscript

although the steady-state $MTR_{asym}$ increases with $T_{1w}$ at relatively low $\omega_1$, the non-steady-state $MTR_{asym}$ acquired with the same $\omega_1$ is roughly insensitive to $T_{1w}$.

## DISCUSSION

Our study suggests that there are two inverse $T_{1w}$ effects ($T_{1w}$ recovery effect and $T_{1w}$-related saturation effect) for the steady-state $MTR_{asym}$. The competition of the two $T_{1w}$ effects results in the complex dependence of $MTR_{asym}$ on $T_{1w}$, which is different from that given by Eq. (2) or Eq. (3) under weak saturation pulse approximation. Since $T_{1w}$-related saturation effect depends on $\omega_1$, $MTR_{asym}$ could be adjusted to be roughly insensitive to $T_{1w}$ by choosing appropriate $\omega_1$. In addition, we show that the non-steady-state $MTR_{asym}$ acquired with very short irradiation time is also roughly insensitive to $T_{1w}$.

In addition to Fig. 1, Fig. 3a shows positive dependence of the steady-state $MTR_{asym}$ on $T_{1w}$, which suggests that the $T_{1w}$ recovery effect may dominate $T_{1w}$-related saturation effect when there are no significant DS effects at high fields or with low irradiation powers. Therefore, in these situations, it is necessary to use $T_{1w}$ normalization to increase the specificity of $MTR_{asym}$. Actually, previous studies at high fields have indicated that $T_{1w}$ normalization is necessary for obtaining specific $MTR_{asym}$ in APT imaging (26,29,30). In contrast, Fig. 3b shows roughly flat curves, which suggests that the two $T_{1w}$ effects are comparable at relatively low fields. For amides at 3.5 ppm at 3 T, $\omega_1$ of 2 μT can satisfy the condition of $\Delta\omega/\omega_1=5$ used in Fig. 3b and thus can make the $MTR_{asym}$ roughly insensitive to $T_{1w}$. In previous APT imaging at 3 T (40), $\omega_1$ from 1 μT–3 μT were traditionally used. Therefore, it may not be necessary to normalize $T_{1w}$ to remove the influence from $T_{1w}$ in some of these previous studies on clinical MRI systems.

Although AREX is equal to the pure CEST effect quantified by $R^{cest}_{ex}$ (26,29,36), the relationship between $MTR_{asym}$ and the pure CEST effect has not been evaluated. Eq. (10) provides an approximate model for $MTR_{asym}$ which provides insight into its contrast sources. Eq. (10) also suggests that $MTR_{asym}R_{1w}/(S_{ref}/S_0)^2$ could be a simple metric to remove the influence from $T_{1w}$ and to obtain relatively purer CEST effects. Simulations in Sup. Fig. S1 show that $MTR_{asym}R_{1w}/(S_{ref}/S_0)^2$ is independent of $T_{1w}$ and is roughly equal to $R^{cest}_{ex}$ except for very strong DS effects. Please note that although we use a two-pool model simulation (Fig. 5) to evaluate Eq. (10), it can be extended to more complex tissue models by inspecting the definition of $S_{ref.}$ Simulations in Sup. Fig. S2 confirm Eq. (10) in a three-pool (solute, semi-solid, and water) model. In biological tissues, $T_{1w}$ also influences $R^{MT}_{ex}$ and thus affects both $S_{ref}$ and $MTR_{asym}$ according to Eq. (9) and Eq. (10). Studies on the influence of $T_{1w}$ on $MTR_{asym}$ through the semi-solid MT effect are also necessary. However, although the analytical equation for $R^{MT}_{ex}$ has been given previously (26), its dependence on $T_{1w}$ is complex. Here, we ignored the semi-solid MT effect in the theoretical analysis, but provided the three-pool model simulated $MTR_{asym}R_{1w}$ and $MTR_{asym}$ vs. $T_{1w}$ in Sup. Fig. S3 and Fig. S4, respectively. Different from the two-pool model simulated $MTR_{asym}$ for higher $\Delta\omega/\omega_1$ (Fig. 3a) or longer $T_{2w}$ (Fig. 3i) which depends on $T_{1w}$, the add of semi-solid MT effect makes $MTR_{asym}$ in these two conditions relatively insensitive to $T_{1w}$. Previously, an empirical $MTR_{asym}$ equation for a two-pool model with DS effect has been also provided (41). Sup. Fig. S5 compares $MTR_{asym}$ in Eq. (10), the empirical

Author Manuscript Author Manuscript Author Manuscript Author Manuscript

$MTR_{asym}$ equation, and the numerical simulated $MTR_{asym}$. It was found that the empirical $MTR_{asym}$ equation matches the numerical simulated $MTR_{asym}$ better than the $MTR_{asym}$ in Eq. (10), suggesting that the empirical $MTR_{asym}$ equation is more accurate than the $MTR_{asym}$ in Eq. (10). However, the empirical $MTR_{asym}$ equation is very complex and is not as straightforward as the $MTR_{asym}$ in Eq. (10) to study the dependence of $MTR_{asym}$ on $T_{1w}$ and DS effect.

In addition to Eq. (1), $MTR_{asym}$ was also defined to be $(S_{ref}(\Delta\omega)-S_{lab}(\Delta\omega))/S_{ref}(\Delta\omega)$ (42,43) which can be looked as the product of $(S_{ref}(\Delta\omega)-S_{lab}(\Delta\omega))/S_0(\Delta\omega)$ and $S_0(\Delta\omega)/S_{ref}(\Delta\omega)$. Here we name this definition as $MTR'_{asym}$. By substituting this definition with Eq. (10), we can obtain,

$$MTR'_{asym}(\Delta\omega) \approx \mathrm{MTR}_{\mathrm{asym}}\frac{S_0}{S_{ref}} \approx \frac{1}{R_{1w}}\frac{S_{ref}}{S_0}R_{ex}^{cest}(\Delta\omega)$$
$$\approx \frac{1}{R_{1w}}\frac{\omega_1^2+\Delta\omega^2}{\frac{R_{2w}}{R_{1w}}\omega_1^2+\Delta\omega^2}R_{ex}^{cest}(\Delta\omega) \qquad (17)$$

Eq. (17) indicates that $MTR'_{asym}$ also has two competing $T_{1w}$ effects, but the influence from the $T_{1w}$-related saturation effect on $MTR'_{asym}$ is relatively weak compared with its influence on $MTR_{asym}$. Therefore, it should require higher $\omega_1$, and thus greater DS effect, for $MTR'_{asym}$ to be roughly insensitive to $T_{1w}$. Sup. Fig. S6 and Fig. S7 show the simulated $MTR'_{asym}R_{1w}$ and $MTR'_{asym}$ vs. $T_{1w}$, respectively, which confirms our expectation. In addition, our analysis is based on CW RF irradiation. For pulsed-RF irradiation, short RF irradiation pulses may also increase the DS effect, which may enhance the $T_{1w}$-related saturation effect.

Heo *et al.* (44) have also studied the dependence of CESTR on $T_{1w}$ for different $\omega_1$ through numerical simulations, and found similar complex dependences: the CESTR at 3.5 ppm increases with $T_{1w}$ under lower $\omega_1$, but is roughly insensitive to $T_{1w}$ or even decreases with $T_{1w}$ under relatively higher $\omega_1$. However, this study did not give an explanation for these complex dependences. Our results about the two competing $T_{1w}$ effects can explain these complex dependences and guide researchers and radiologists to choose appropriate quantification metrics. Previously, Jokivarsi *et al.* (45) showed a strong correlation between $MTR_{asym}$ and pH in ischemic stroke. However, Sun *et al.* (45) showed that the correlation between $MTR_{asym}/T_{1w}$ and pH is stronger than that between $MTR_{asym}$ and pH in ischemic stroke. Based on our study, choosing an appropriate CEST quantification metric should consider the relative contributions of the two $T_{1w}$ effects for specific experimental conditions.

Fig. 6 and Fig. 8 suggest that the non-steady-state $MTR_{asym}$ with very short RF irradiation time and long recovery time is roughly insensitive to $T_{1w}$ effect. This may be due to the different dynamics of chemical exchange, $T_{1w}$ recovery, and $T_{1w}$-related saturation effects. Based on the Bloch equations with exchange terms (3), the water signal depends on three terms including the chemical exchange term ($M_{zw}k_{ws}$, where $M_{zw}$ is the water Z

Author Manuscript Author Manuscript Author Manuscript Author Manuscript

magnetization and $k_{ws}$ is the rate of exchange from water to solute protons, and in which we ignore the small back exchange), $T_{1w}$ recovery term ($R_{1w}(M_{0w} - M_{zw})$, where $M_{0w}$ is the equilibrium water magnetization), and water saturation term ($\omega_1 M_{yw}$, where $M_{yw}$ is the water Y magnetization). In a short time after the irradiation, both $M_{zw} - M_{0w}$ and $M_{yw}$ are very small, but $M_{zw}$ is large. Thus chemical exchange dominates other two $T_{1w}$ effects, and as a result $MTR_{asym}$ is insensitive to $T_{1w}$. Fig. 7 suggests that the non-steady-state $MTR_{asym}$ with very short RF irradiation time and short recovery time is also roughly insensitive to $T_{1w}$ effect. This may be due to that the dependences of the labeled signal, the reference signal, and the non-equilibrium control signal on $T_{1w}$ are roughly the same, and thus could be cancelled. However, when equilibrium control signal is used, the non-steady-state $MTR_{asym}$ with very short RF irradiation time and short recovery time is still influenced by $T_{1w}$ (Sup. Fig. S8).

Although steady-state $MTR_{asym}$ can be adjusted to be roughly insensitive to $T_{1w}$, the direct subtraction of the label and reference signals cannot remove the higher order effect of the influence from the semi-solid MT effect. In situations, such as tumor, where there is significant change of semi-solid MT effect (46), $MTR_{asym}$ may be still contaminated by the semi-solid MT effect. Variation of $T_{1w}$ is usually associated with multiple physiological parameters such as water content. A recent paper indicates that the increase of $T_{1w}$ could be mostly eliminated by the increase of water content in tumors (47). This study is important for interpretation of contrast mechanism in many CEST applications. In this paper, we ignore this dependence and only studied the specificity of $MTR_{asym}$ to solute concentration from a perspective of theory.

## CONCLUSION

We show that $MTR_{asym}$ has different dependences on $T_{1w}$ at high fields, low fields, and with steady-state or non-steady-state acquisitions. For some previous studies on clinical MRI systems with appropriate sequence parameters, the steady-state $MTR_{asym}$ may be roughly insensitive to $T_{1w}$; For non-steady state acquisitions with very short RF irradiation time, $MTR_{asym}$ is also roughly insensitive to $T_{1w}$.

## Supplementary Material

Refer to Web version on PubMed Central for supplementary material.

## Abbreviations used

| | |
|---|---|
| **CEST** | chemical exchange saturation transfer |
| **APT** | amide proton transfer |
| **MT** | magnetization transfer |
| **MTR** | magnetization transfer ratio |
| **$MTR_{asym}$** | magnetization transfer ratio with asymmetric analysis |
| **AREX** | apparent exchange-dependent relaxation |

Author Manuscript Author Manuscript Author Manuscript Author Manuscript

| | |
|---|---|
| **DS** | direct water saturation |
| $\mathbf{R_{1\rho}}$ | water longitudinal relaxation rate in the rotating frame |
| $\mathbf{R^{cest}ex}$ | chemical exchange effect in the rotating frame |
| $\mathbf{R^{MT}ex}$ | semi-solid magnetization transfer effect in the rotating frame |

## REFERENCES


1. van Zijl PCM , Yadav NN . Chemical Exchange Saturation Transfer (CEST): What is in a Name and What Isn't? Magnetic Resonance in Medicine 2011;65(4):927–948.21337419
2. van Zijl PCM , Zhou J , Mori N , et al. Mechanism of magnetization transfer during on-resonance water saturation. A new approach to detect mobile proteins, peptides, and lipids. Magnetic Resonance in Medicine 2003;49(3):440–449.12594746
3. Zhou JY , van Zijl PCM . Chemical exchange saturation transfer imaging and spectroscopy. Progress in Nuclear Magnetic Resonance Spectroscopy 2006;48(2–3):109–136.
4. Walker-Samuel S , Ramasawmy R , Torrealdea F , et al. In vivo imaging of glucose uptake and metabolism in tumors. Nature Medicine 2013;19(8):1067–1074.
5. Zhou JY , Tryggestad E , Wen ZB , et al. Differentiation between glioma and radiation necrosis using molecular magnetic resonance imaging of endogenous proteins and peptides. Nature Medicine 2011;17(1):130–U308.
6. Cai KJ , Haris M , Singh A , et al. Magnetic resonance imaging of glutamate. Nature Medicine 2012;18(2):302–306.
7. Cai KJ , Tain RW , Zhou XJ , et al. Creatine CEST MRI for Differentiating Gliomas with Different Degrees of Aggressiveness. Mol Imaging Biol 2016;19(2):225–232.
8. Haris M , Cai KJ , Singh A , Hariharan H , Reddy R . In vivo mapping of brain myo-inositol. Neuroimage 2011;54(3):2079–2085.20951217
9. Zaiss M , Kunz P , Goerke S , Radbruch A , Bachert P . MR imaging of protein folding in vitro employing Nuclear-Overhauser-mediated saturation transfer. Nmr in Biomedicine 2013;26(12): 1815–1822.24115020
10. Zhang XY , Wang F , Jin T , et al. MR imaging of a novel NOE-mediated magnetization transfer with water in rat brain at 9.4T. Magnetic Resonance in Medicine 2017;78(2):588–597.27604612
11. Liu GS , Ali MM , Yoo B , et al. PARACEST MRI With Improved Temporal Resolution. Magnetic Resonance in Medicine 2009;61(2):399–408.19165903
12. Chen LQ , Howison CM , Jeffery JJ , et al. Evaluations of Extracellular pH within In Vivo Tumors Using acidoCEST MRI. Magnetic Resonance in Medicine 2014;72(5):1408–1417.24281951
13. Ward KM , Balaban RS . Determination of pH using water protons and chemical exchange dependent saturation transfer (CEST). Magnetic Resonance in Medicine 2000;44(5):799–802.11064415
14. Zhou JY , Payen JF , Wilson DA , Traystman RJ , van Zijl PCM . Using the amide proton signals of intracellular proteins and peptides to detect pH effects in MRI. Nature Medicine 2003;9(8): 1085–1090.
15. Salhotra A , Lal B , Laterra J , et al. Amide proton transfer imaging of 9L gliosarcoma and human glioblastoma xenografts. Nmr in Biomedicine 2008;21(5):489–497.17924591
16. Jones CK , Schlosser MJ , van Zijl PCM , et al. Amide proton transfer imaging of human brain tumors at 3T. Magnetic Resonance in Medicine 2006;56(3):585–592.16892186
17. Jia GA , Abaza R , Williams JD , et al. Amide Proton Transfer MR Imaging of Prostate Cancer: A Preliminary Study. Journal of Magnetic Resonance Imaging 2011;33(3):647–654.21563248
18. Zhou JY , Lal B , Wilson DA , Laterra J , van Zijl PCM . Amide proton transfer (APT) contrast for imaging of brain tumors. Magnetic Resonance in Medicine 2003;50(6):1120–1126.14648559
19. Sun PZ , Wang EF , Cheung JS . Imaging acute ischemic tissue acidosis with pH-sensitive endogenous amide proton transfer (APT) MRI-Correction of tissue relaxation and concomitant RF

Author Manuscript Author Manuscript Author Manuscript Author Manuscript

irradiation effects toward mapping quantitative cerebral tissue pH. Neuroimage 2012;60(1):1–6.22178815

20. Sun PZ , Zhou JY , Sun WY , Huang J , van Zijl PCM . Detection of the ischemic penumbra using pH-weighted MRI. Journal of Cerebral Blood Flow and Metabolism 2007;27(6):1129–1136.17133226
21. Sun PZ , Benner T , Copen WA , Sorensen AG . Early Experience of Translating pH-Weighted MRI to Image Human Subjects at 3 Tesla. Stroke 2010;41(10):S147–S151.20876492
22. Li H , Zu ZL , Zaiss M , et al. Imaging of amide proton transfer and nuclear Overhauser enhancement in ischemic stroke with corrections for competing effects. Nmr in Biomedicine 2015;28(2):200–209.25483870
23. Dula AN , Asche EM , Landman BA , et al. Development of Chemical Exchange Saturation Transfer at 7T. Magnetic Resonance in Medicine 2011;66(3):831–838.21432902
24. Zhang H , Wang WZ , Jiang SS , et al. Amide proton transfer-weighted MRI detection of traumatic brain injury in rats. Journal of Cerebral Blood Flow and Metabolism 2017;37(10):3422–3432.28128026
25. Wang WZ , Zhang H , Lee DH , et al. Using functional and molecular MRI techniques to detect neuroinflammation and neuroprotection after traumatic brain injury. Brain Behavior and Immunity 2017;64:344–353.
26. Zaiss M , Zu ZL , Xu JZ , et al. A combined analytical solution for chemical exchange saturation transfer and semi-solid magnetization transfer. Nmr in Biomedicine 2015;28(2):217–230.25504828
27. Zaiss M , Bachert P . Exchange-dependent relaxation in the rotating frame for slow and intermediate exchange - modeling off-resonant spin-lock and chemical exchange saturation transfer. Nmr in Biomedicine 2013;26(5):507–518.23281186
28. Zaiss M , Xu JZ , Goerke S , et al. Inverse Z-spectrum analysis for spillover-, MT-, and T-1-corrected steady-state pulsed CEST-MRI - application to pH-weighted MRI of acute stroke. Nmr in Biomedicine 2014;27(3):240–252.24395553
29. Zaiss M , Xu J , Goerke S , et al. Inverse Z-spectrum analysis for spillover, MT-, and T1-corrected steady-state pulsed CEST-MRI-application to pH-weighted MRI of acute stroke. Nmr in Biomedicine 2014;27(3):240–252.24395553
30. Li H , Li K , Zhang XY , et al. R-1 correction in amide proton transfer imaging: indication of the influence of transcytolemmal water exchange on CEST measurements. Nmr in Biomedicine 2015;28(12):1655–1662.26466161
31. Yuan J , Chen SZ , King AD , et al. Amide proton transfer-weighted imaging of the head and neck at 3 T: a feasibility study on healthy human subjects and patients with head and neck cancer. Nmr in Biomedicine 2014;27(10):1239–1247.25137521
32. Heo HY , Zhang Y , Lee DH , et al. Accelerating chemical exchange saturation transfer (CEST) MRI by combining compressed sensing and sensitivity encoding techniques. Magnetic Resonance in Medicine 2017;77(2):779–786.26888295
33. Heo HY , Zhang Y , Jiang SS , Lee DH , Zhou JY . Quantitative Assessment of Amide Proton Transfer (APT) and Nuclear Overhauser Enhancement (NOE) Imaging with Extrapolated Semisolid Magnetization Transfer Reference (EMR) Signals: II. Comparison of Three EMR Models and Application to Human Brain Glioma at 3 Tesla. Magnetic Resonance in Medicine 2016;75(4):1630–1639.26033553
34. Heo HY , Zhang Y , Burton TM , et al. Improving the Detection Sensitivity of pH-Weighted Amide Proton Transfer MRI in Acute Stroke Patients Using Extrapolated Semisolid Magnetization Transfer Reference Signals. Magnetic Resonance in Medicine 2017;78:871–880.28639301
35. Ma XY , Bai Y , Lin YS , et al. Amide proton transfer magnetic resonance imaging in detecting intracranial hemorrhage at different stages: a comparative study with susceptibility weighted imaging. Scientific Reports 2017;7.
36. Zaiss M , Bachert P . Chemical exchange saturation transfer (CEST) and MR Z-spectroscopy in vivo: a review of theoretical approaches and methods. Physics in Medicine and Biology 2013;58(22):R221–R269.24201125

Author Manuscript Author Manuscript Author Manuscript Author Manuscript

37. Zaiss M , Angelovski G , Demetriou E , et al. QUESP and QUEST Revisited - fast and accurate quantitative CEST experiments. Magn Reson Med 2017:DOI: 10.1002/mrm.26813.

38. Goerke S , Zaiss M , Bachert P . Characterization of creatine guanidinium proton exchange by water-exchange (WEX) spectroscopy for absolute- pH CEST imaging in vitro. Nmr in Biomedicine 2014;27(5):507–518.24535718

39. Sun PZ , Benner T , Kumar A , Sorensen AG . Investigation of optimizing and translating pH-sensitive pulsed-chemical exchange saturation transfer (CEST) imaging to a 3T clinical scanner. Magnetic Resonance in Medicine 2008;60(4):834–841.18816867

40. Zhao XN , Wen ZB , Huang FH , et al. Saturation Power Dependence of Amide Proton Transfer Image Contrasts in Human Brain Tumors and Strokes at 3 T. Magnetic Resonance in Medicine 2011;66(4):1033–1041.21394783

41. Sun PZ , van Zijl PCM , Zhou JY . Optimization of the irradiation power in chemical exchange dependent saturation transfer experiments. Journal of Magnetic Resonance 2005;175(2):193–200.15893487

42. McMahon MT , Gilad AA , Zhou JY , et al. Quantifying exchange rates in chemical exchange saturation transfer agents using the saturation time and saturation power dependencies of the magnetization transfer effect on the magnetic resonance imaging signal (QUEST and QUESP): pH calibration for poly-L-lysine and a starburst dendrimer. Magnetic Resonance in Medicine 2006;55(4):836–847.16506187

43. Wermter FC , Bock C , Dreher W . Investigating GluCEST and its specificity for pH mapping at low temperatures. Nmr in Biomedicine 2015;28(11):1507–1517.26412088

44. Heo HY , Lee DH , Zhang Y , et al. Insight into the quantitative metrics of chemical exchange saturation transfer (CEST) imaging. Magnetic Resonance in Medicine 2017;77(5):1853–1865.27170222

45. Jokivarsi KT , Grohn HI , Grohn OH , Kauppinen RA . Proton transfer ratio, lactate, and intracellular pH in acute cerebral ischemia. Magnetic Resonance in Medicine 2007;57(4):647–653.17390356

46. Xu JZ , Li K , Zu ZL , et al. Quantitative magnetization transfer imaging of rodent glioma using selective inversion recovery. NMR in Biomedicine 2014;27(3):253–260.24338993

47. Lee DH , Heo HY , Zhang K , et al. Quantitative assessment of the effects of water proton concentration and water T-1 changes on amide proton transfer (APT) and nuclear overhauser enhancement (NOE) MRI: The origin of the APT imaging signal in brain tumor. Magnetic Resonance in Medicine 2017;77(2):855–863.26841096

Author Manuscript Author Manuscript Author Manuscript Author Manuscript

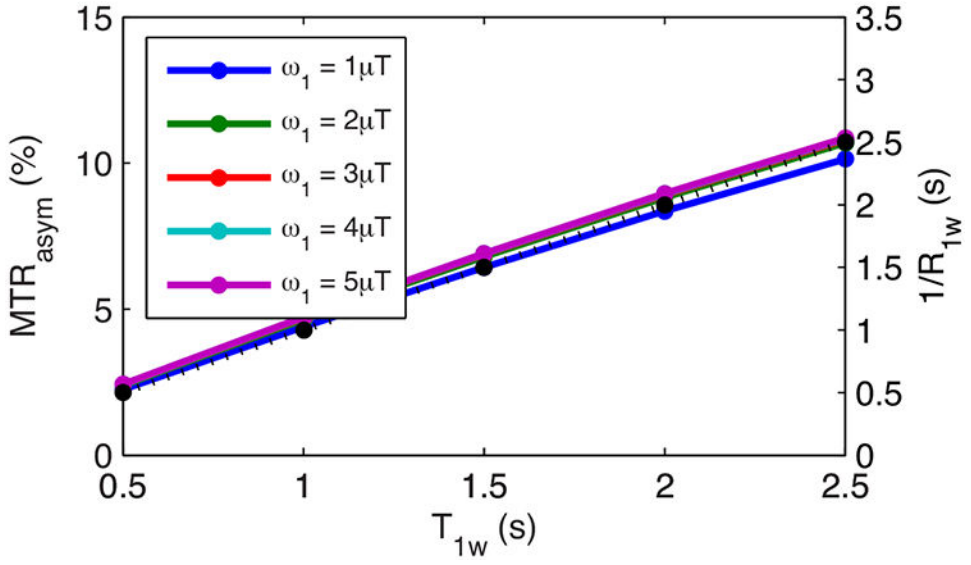


**FIG. 1.**

Steady-state $MTR_{asym}$ vs. $T_{1w}$ for $\omega_1 << \Delta\omega$ ($\Delta\omega/\omega_1=100$) with a series of $\omega_1$ (solid lines) as well as $1/R_{1w}$ vs. $T_{1w}$ (dotted line). Note that the lines with different $\omega_1$ are indicated by different colors, which overlap. Also note that the solid lines and the dotted line overlap.

Author Manuscript Author Manuscript Author Manuscript Author Manuscript

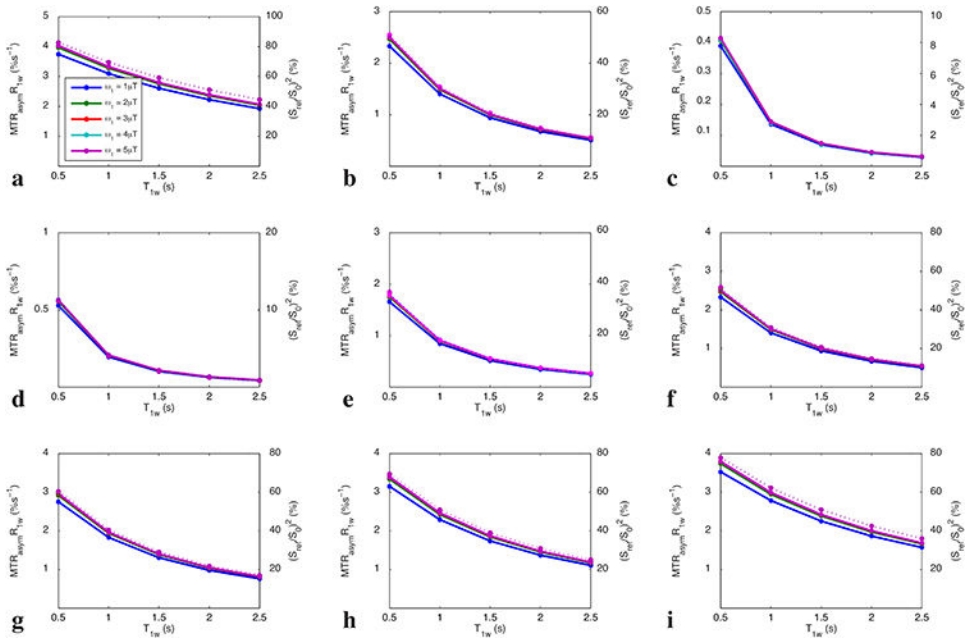

**FIG. 2.**

Steady-state $MTR_{asym}R_{1w}$ vs. $T_{1w}$ for $\Delta\omega/\omega_1$=10, 5, and 2 with $T_{2w}$ of 50 ms (a-c), as well as for $T_{2w}$ = 10 ms, 30 ms, 50 ms, 70 ms, 100 ms, and 150 ms with $\Delta\omega/\omega_1$=5 (d-i). Solid lines represent the simulated $MTR_{asym}R_{1w}$, and the dotted line represents the simulated $(S_{ref}/S_0)^2$. Note that the lines with different $\omega_1$ are indicated by different colors, which overlap. Also note that the solid lines and the dotted line overlap.

Author Manuscript Author Manuscript Author Manuscript Author Manuscript

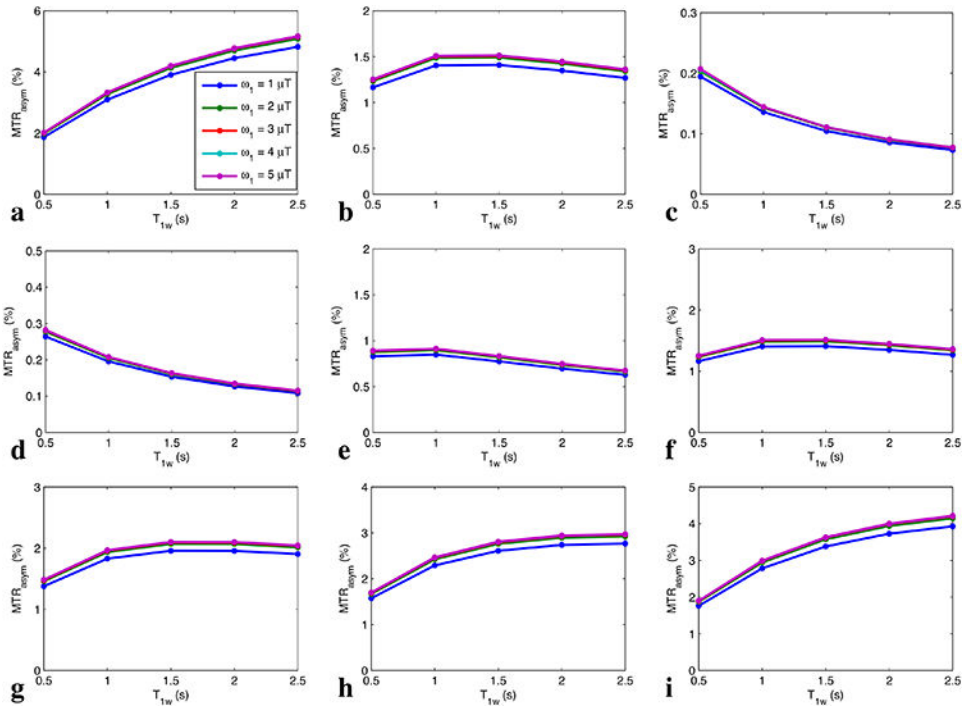


**FIG. 3.**

Steady-state $MTR_{asym}$ vs. $T_{1w}$ for $\Delta\omega/\omega_1$=10, 5, and 2 with $T_{2w}$ of 50 ms (a-c), as well as for $T_{2w}$ = 10 ms, 30 ms, 50 ms, 70 ms, 100 ms, and 150 ms with $\Delta\omega/\omega_1$=5 (d-i). Note that the lines with different $\omega_1$ are indicated by different colors, which overlap.

Author Manuscript Author Manuscript Author Manuscript Author Manuscript

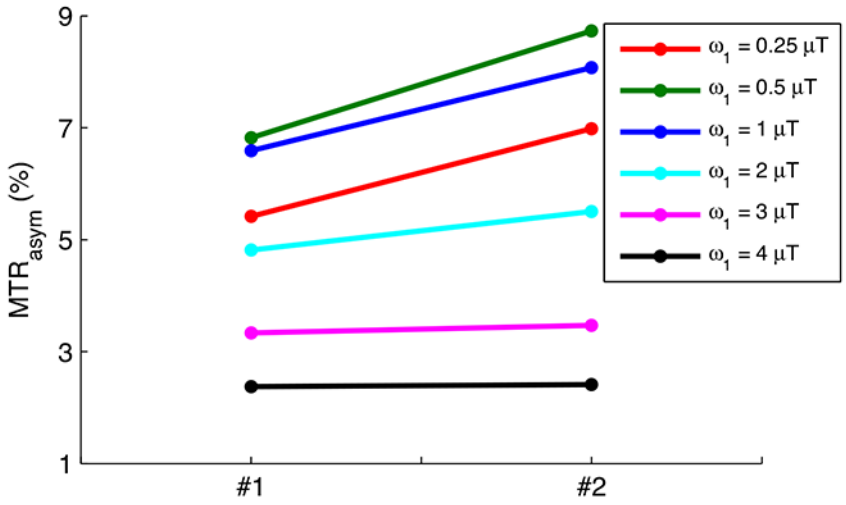


**FIG. 4.**

Measured steady-state $MTR_{asym}$ from two creatine samples with different $T_{1w}$. $T_{1w}$ and $T_{2w}$ were measured to be (0.9 s and 88 ms) and (1.2 s and 132 ms) for sample #1 and #2, respectively.

Author Manuscript Author Manuscript Author Manuscript Author Manuscript

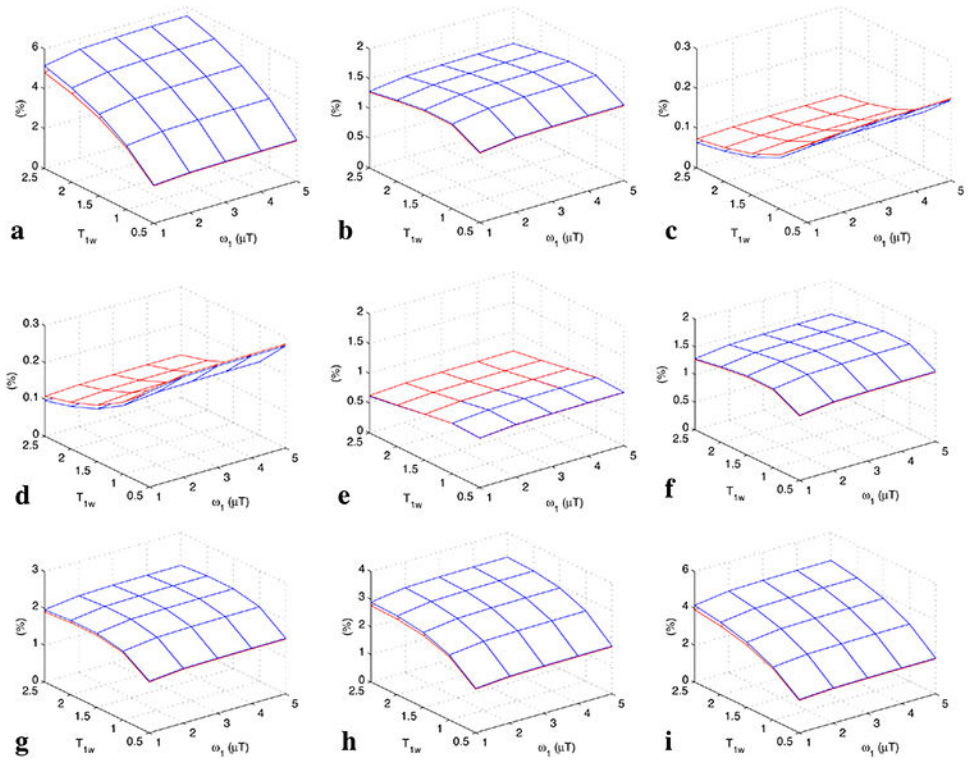


**FIG. 5.**

Steady-state $MTR_{asym}$ (red) and $(S_{ref}/S_0)^2 R^{cest}_{ex}/R_{1w}$ (blue) vs. $T_{1w}$ for $\Delta\omega/\omega_1$=10, 5, and 2 with $T_{2w}$ of 50 ms (a-c), as well as for $T_{2w}$ = 10 ms, 30 ms, 50 ms, 70 ms, 100 ms, and 150 ms with $\Delta\omega/\omega_1$=5 (d-i).

Author Manuscript Author Manuscript Author Manuscript Author Manuscript

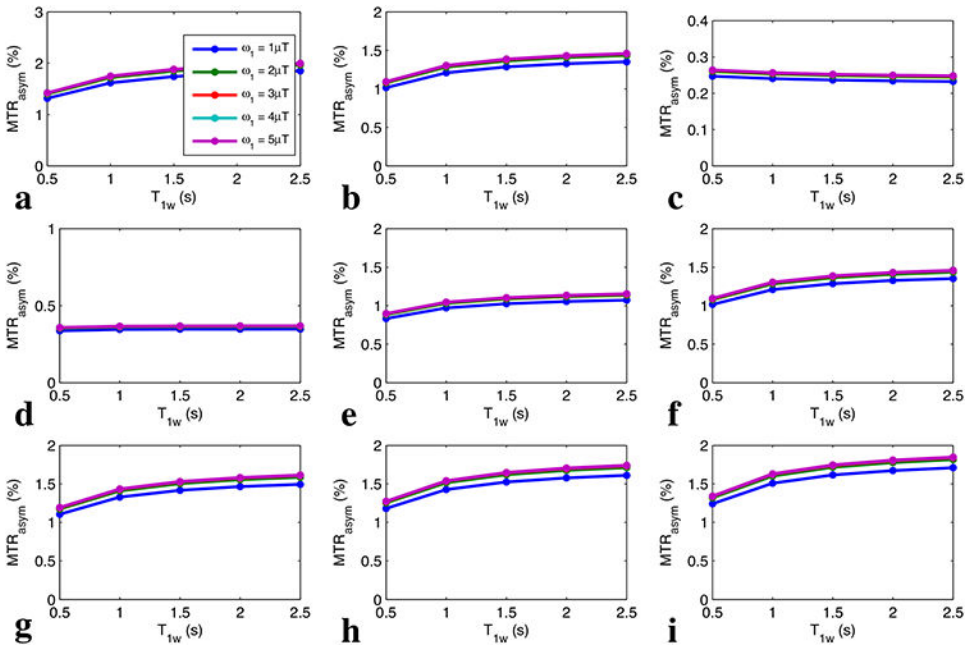


**FIG. 6.**

Non-steady-state $MTR_{asym}$ with full recovery vs. $T_{1w}$ for $\Delta\omega/\omega_1$=10, 5, and 2 with $T_{2w}$ of 50 ms (a-c), as well as for $T_{2w}$ = 10 ms, 30 ms, 50 ms, 70 ms, 100 ms, and 150 ms with $\Delta\omega/\omega_1$=5 (d-i). Note that the lines with different $\omega_1$ are indicated by different colors, which overlap.

Author Manuscript Author Manuscript Author Manuscript Author Manuscript

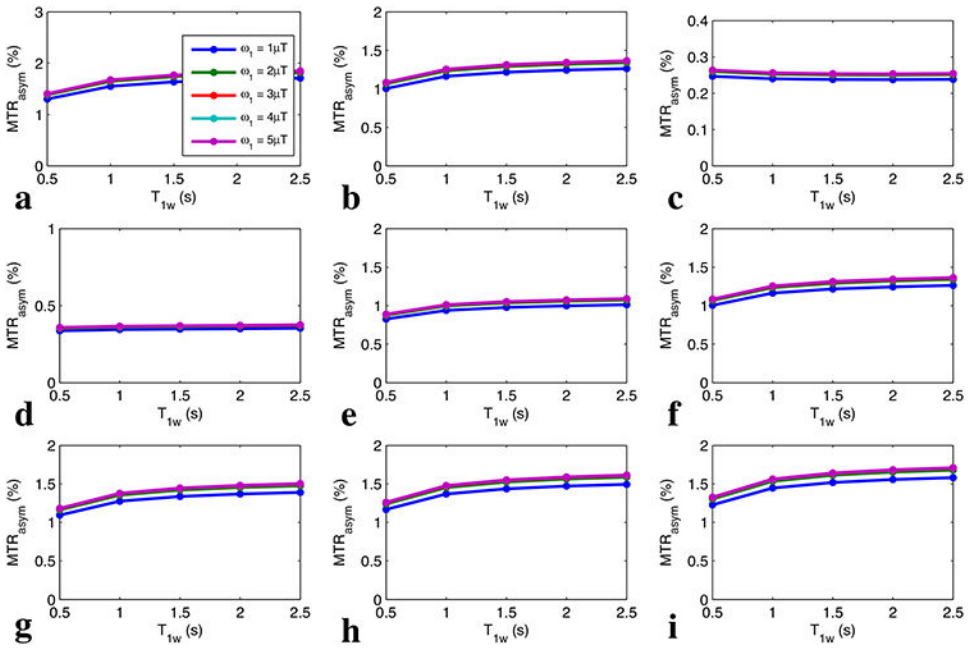


**FIG. 7.**

Non-steady-state $MTR_{asym}$ with short recovery time vs. $T_{1w}$ for $\Delta\omega/\omega_1$=10, 5, and 2 with $T_{2w}$ of 50 ms (a-c), as well as for $T_{2w}$ = 10 ms, 30 ms, 50 ms, 70 ms, 100 ms, and 150 ms with $\Delta\omega/\omega_1$=5 (d-i). Note that the lines with different $\omega_1$ are indicated by different colors, which overlap.

Author Manuscript Author Manuscript Author Manuscript Author Manuscript

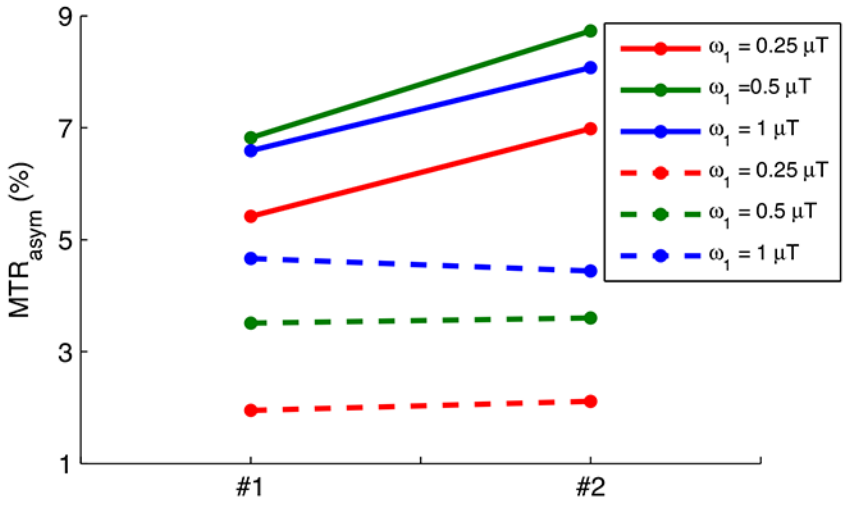


**FIG. 8.**

Measured steady-state (solid lines) and non-steady-state (dashed lines) $MTR_{asym}$ from two creatine samples with different $T_{1w}$. $T_{1w}$ and $T_{2w}$ were measured to be (0.9 s and 88 ms) and (1.2 s and 132 ms) for sample #1 and #2, respectively.

Author Manuscript

Author Manuscript

Author Manuscript

Author Manuscript

**Table 1.**

Parameters for the two-pool model numerical simulations with pool concentration (f), exchange rate (k), longitudinal relaxation time ($T_1$), transverse relaxation time ($T_2$), and resonance frequency offset for each pool ($\Delta_r$). Water content is set to be 1.

| | f | k ($s^{-1}$) | $T_1$ (s) | $T_2$ (ms) | $\Delta_r$ (ppm) |
|---|---|---|---|---|---|
| Solute | 0.001 | 50 | 1.5 | 15 | - |
| Water | 1 | - | 0.5, 1, 1.5, 2, 2.5 | 50 | 0 |